INSTITUTE
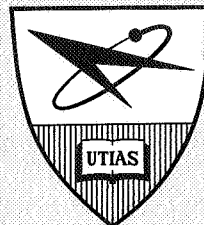
FOR

AEROSPACE STUDIES

UNIVERSITY OF TORONTO

SEMI ANNUAL STATUS REPORT

NASA RESEARCH GRANT NGR -52-026-011

Covering Period July 25th, 1966 to Present

by

R. C. Tennyson

April 18th, 1967.

BUCKLING OF CIRCULAR CYLINDRICAL SHELLS
IN AXIAL COMPRESYION

A.   Buckling of Photoelastic Circular Cylinders in Axial Compression

Circular cylindrical photoelastic shells having radius–to–thickness ratios varying from 100 to 600 have been successfully spun-cast in the rotation apparatus shown in Fig. **H-6.1**   Tolerances on the shell wall thickness have generally averaged about $\pm$ 3%. The cylinders were found to buckle within 10% to 14% of the classical value, or within only a few percent of the reduced value taking into account the effect of clamped end constraints (see **Fig. H-6.2**). Each buckling load was repeatable as many as twenty times, and the behaviour of the cylinders was completely elastic. The addition of strain gauges to the thinner walled shells was found to significantly stiffen the local wall area, thus yielding high values for the modulus of elasticity. As a result, recourse was had to determining the modulus by measuring the axial end deformation with dial gauges (accurate to 0.0001 in.) and by photoelastic observation of the change in fringe order with load.

Several of the photoelastic shells were **used** to study the snap-through buckling process. The shells were illuminated by two high intensity continuous lamps each with a linear polarizer set at 45° attached to the housing. Both Fastax and Hycam 16 mm high speed cameras were employed to record the change in the 45° isoclinic pattern during the buckling process. The experimental set-up is **shown** in Fig. **H-6.3,**

In an earlier **experimental investigation** of the buckling process, **the** 45°

isoclinic patterns were photographed in a close-up view of a cylinder which buckled into a single tier as shown in Fig. H-6.4. However, in this investigation the complete cylinder length was photographed and observed to buckle into two tiers, Figures H-6.5 and H-6.6 present a few of the results obtained and the following observations can be made.

Buckling began at an isolated location on the shell in Fig. H-6.5 at a critical buckling load ratio $(P_{cr}/P_{cl}) \approx 0.90$; and rapidly spread both axially and circumferentially. In frame (8, 1) of the 9 x 3 picture matrix in Fig. H-6.5, three tiers of buckles are visible, with buckles in a more advanced stage appearing in the second and third tiers. However, at the inception of buckling in the remainder of the shell, the isoclinic patterns bear a strong resemblance to that of frame (3, 1) in Fig. H-6.4. As demonstrated in UTIAS Report No. 102, the square wave classical mode shape yields a 45° isoclinic pattern very similar to frame (3, 1).

The axisymmetric isoclinic rings, which are particularly visible in frames (2, 2) to (4, 3) in Fig. H-6.5, correspond to the axisymmetric buckling mode which has also been found to satisfy the classical equations of equilibrium. It is evident that these rings appear first, with the asymmetric buckling mode (i.e. the square wave pattern) following (eg: see frames (4, 2) to (7, 2)). A complete analysis of the theoretical isoclinic patterns corresponding to various buckling mode shapes and a comparison with high speed photographs of the 45° isoclinics will be **available** in a subsequent UTIAS publication.

B.   The Effects of Cutouts in Photoelastic Circular Cylinders under
            Axial Compression

Circular cylindrical shells represent the primary load carrying structure of high speed aircraft, launch vehicles and many other aerospace systems. Structural discontinuities in the form of cutouts are inevitable and little is known about them in

cylinders, both experimentally and theoretically. The effect of circular, elliptical and rectangular cutouts on the stress distribution, the buckling load and buckling mode shapes is being analyzed experimentally using photoelastic plastic cylinders. Presently, only the case of axial. compression of cylinders with circular cutouts has been considered.

The photoelastic shells were manufactured using the spin-casting apparatus shown in Fig. H-6. 1. In order to produce cutouts in the cylinder wall without inducing residual stresses at the free edge, a small grinding wheel mounted on a high speed 'Dremel' motor was used. The holes were first 'rough-cut' to the desired shape and then careful sanding was employed to complete the cutout. Circular holes of radii 0. 128", 0. 500" and 0. 625" have been fabricated in two cylinders to-date (see Fig. H-7. 1).

Lurie first proposed a solution to the problem of the stress distribution for a circular hole in a circular cylinder subjected to axial tension (or cornpression). However, the solution was restricted to very small holes in shallow shells for which $a^2/Rt \ll 1$, where a is the hole radius, R is the radius of curvature of the cylinder's mid surface and t is the shell wall thickness. Subsequent investigation by Van Dyke yielded a numerical solution for the same problem, only for much larger values of the curvature parameter β, where $\beta^2 = a^2 \left[12(1-\nu^2) \right]^{1/2}/8\,Rt$ and $\nu =$ Poisson's ratio. In the limiting case of $\beta \to 0$, the flat plate solution was obtained.

Figure H-7. 2 shows the 0°, 90° isoclinic patterns for a circular hole for which $\beta = 0.196$. The stress distribution along the X and Y axes (refer to Fig. H-7. 3) was determined from photoelastic measurements and the results are contained in Fig. H-7. 4 and Fig. H-7. 5. Currently, stress distributions for a wide range of β are being compiled and the results compared with the theoretical values computed by Van Dyke.

APPENDIX

Analysis of the Buckling Process of Circular Cylindrical Shells under Axial Compression

The material contained in this appendix summarizes very briefly the contents of a UTIAS report which is to be published shortly. The **work** outlined in Part A of the status report has now been successfully completed and it has been shown that the theoretical mode shapes assumed by the shell both at the inception of and during the buckling process were observed experimentally in the form of changing 45° isoclinic patterns (see for example, Figs. **H-6.4, H-6.** 5, **H-6. 6**).

Theoretical Analysis of the Classical Linear Buckling Mode 45° Isoclinics

The classical linear compatibility equation **for** a circular cylindrical shell element is

$$\nabla^4 F + \frac{E}{R} w_{,xx} = 0 \tag{1}$$

Assume a radial deflection mode shape defined by Koiter, which represents **a** sufficiently general shape at the inception of buckling, of the form

$$w(x,y) = -w + w_0 \cos\frac{p_0 x}{R} + w_{mn} \cos\frac{px}{R} \cos\frac{ny}{R} \tag{2}$$

Substituting eq. (2) into eq. (1) yields

$$F(x,y) = -\left[f_0 \cos\frac{p_0 x}{R} + f_{mn} \cos\frac{px}{R} \cos\frac{ny}{R} + \frac{\sigma_x}{2} y^2 \right] \tag{3}$$

If eqs. (2) and (3) are substituted into eq. (1) and the coefficients of the trigonometric functions compared, the stress function coefficients become,

$$f_0 / w_0 = -\dot{E}R / p_0^2$$

$$f_{mn} / w_{mn} = -ER\, p^2 / (p^2 + n^2)^2 \tag{4}$$

or $f_m / w_{mn} = - ER/p_o^2$ since the classical buckling case requires

$$p^2 - p_o p + n^2 = 0 \qquad (5)$$

The 45° isoclinic equation in terms of stress functions can be written in the form,

$$F_{,yy} - F_{,xx} = 0 \qquad (6)$$

for F, xy $\neq$ 0

Substituting eqs. (3) and (4) into eq. (6) and noting from Koiter's work

that $\qquad w_{mn} = 2 w_o p_o / n$

$$(7)$$

one obtains

$$\cos p_o \frac{x}{R} + \frac{2}{p_o n} (p^2 - n^2) \cos \frac{px}{R} \cos \frac{ny}{R} = \frac{\sigma_x R}{w_o E} \qquad (8)$$

which defines the 45° isoclinic equation at the inception of buckling.

For the case when $p = n$, eq. (8) reduces to

$$\cos p_o \frac{x}{R} = \frac{\sigma_x R}{w_o E} \qquad (9)$$

Hence axisymmetric rings will define the 45° isoclinics separated by a distance $\frac{2\pi R}{p_o}$, The presence of axisymmetric isoclinic rings in frames (2, 2) to (7, 2) of Fig. **H-6.5** at the onset of buckling is therefore predicted by theory. Furthermore, it was found that the separation distance between the isoclinic rings agrees within a few percent of the theoretical value $2\pi R/p_o$.

When $p \neq n$, eq. **(8)** plots in the form of an ellipse or oval shaped isoclinic. These later forms of the 45° isoclinics are observed after the rings begin to vanish, (see for example frames (3, 2) and (4, 2) of Fig. H-6.5).

Theoretical Analysis of the Nonlinear Postbuckling Mode 45° Isoclinics

The nonlinear form of the compatibility equation used to-date in the study of the postbuckling behaviour of cylindrical shells is

$$\nabla^4 F / E = W_{,xy}^2 - W_{,xx} W_{,yy} - \frac{W_{,xx}}{R} \tag{10}$$

As a first-approximation to a radial deflection function, which is presumed to adequately describe the buckled mode shape beyond **eq. (2),** assume

$$w(X,Y) = -W_{00} + W_{11} \cos \pi X \cos \pi Y + W_{20} \cos 2\pi X$$
$$+ W_{02} \cos 2\pi Y \tag{11}$$

where $X = \dfrac{x}{l_x}$, $Y = \dfrac{y}{l_y}$

Substituting eq. (11) into eq. (10) yields a stress function of the form,

$$F(X,Y) = - \left[f_{11} \cos \pi X \cos \pi Y + f_{22} \cos 2\pi X \cos 2\pi Y \right.$$
$$+ f_{13} \cos \pi X \cos 3\pi Y + f_{31} \cos 3\pi X \cos \pi Y + f_{20} \cos 2\pi X$$
$$\left. + f_{02} \cos 2\pi Y + \frac{\sigma_x}{2} \left(\frac{\pi R Y}{n} \right)^2 \right] \tag{12}$$

Again, the stress function coefficients can be evaluated by substituting eqs. (11) and (12) into eq. (10) and comparing coefficients of the trigonometric functions. viz:

$$f_{11} = \frac{2 E W_{11} \mu^2}{(1+\mu^2)^2} \left(W_{20} + W_{02} - \frac{l_y^2}{2\pi^2 R} \right)$$

$$f_{22} = \frac{E W_{02} W_{20} \mu^2}{(1+\mu^2)^2}$$

$$f_{13} = \frac{2 E W_{11} W_{02} \mu^2}{(9+\mu^2)^2}$$

$$f_{31} = \frac{2 E W_{11} W_{20} \mu^2}{(1+9\mu^2)^2} \tag{13}$$

$$f_{20} = \frac{E W_{11}^2}{32 \mu^2} \left(1 - \frac{8 l_y^2 W_{20}}{\pi^2 R W_{11}^2} \right)$$

$$f_{02} = \frac{E W_{11}^2 \mu^2}{32}$$

where $\mu = l_y / l_x$.

Substituting eqs. (12) and (13) into the 45° isoclinic equation (eq. (6)) one obtains,

$$2 f_{13} \cos \pi X \cos 3\pi Y - 2 f_{31} \cos 3\pi X \cos \pi Y$$
$$+ f_{02} \cos 2\pi Y - f_{20} \cos 2\pi X = \frac{\sigma_x l^2}{4\pi^2} \tag{14}$$

for the case when $\mu = 1$ (ie; $l_y = l_x = l$ say.)

From Hoff's paper in which the radial deflection coefficients were obtained for various terms in the Fourier series expansion, it was observed that

$$\begin{aligned}
w_{11} / t &\simeq 6.8 \\
w_{02} / t &\simeq 0 \\
w_{20} / t &\simeq 2.38
\end{aligned} \tag{15}$$

which were invariant with values of μ .

It is shown in the **UTIAS** report to be published that eq. (14) with the aid of eqs. (13) and (15) plots an isoclinic shape having the form of frames (1, 1) to (3, 1) of Fig. **H-6.4**, Since that buckling series represented single tier buckling, it is interesting to compare these latter results with the multi-tier buckling series **of** Fig. **H-6.5**. In particular, it is observed in many tests, including the results **of** Fig. **H-6.5**, that the double-diamond shaped isoclinic patterns emerge in the latter stages of buckling, independent of the state of the buckling process at adjacent locations. In other words, there is a fundamental mode shape change that must occur as the shell passes through the unstable states toward its large-displacement equilibrium configuration. This mode shape is adequately described by eq. (11) (ie: Kempner's mode shape).

It is also interesting to conjecture that by adding more terms in the Fourier series description of the radial deflection function, a multi-valued solution

of eq. (6) will not result. However, multi-valued solutions are necessary since at the later stages of the postbuckling photographs, more than one isoclinic pattern is required to characterize the mode shape (see for example Fig. H-6.6 or frames (4, 1), etc. of Fig. H-6.4). Consequently, the compatibility equation and the equilibrium equation used to describe postbuckling behaviour are probably not sufficiently general enough to characterize the shell deformation beyond the early stages of initial buckling. This result was also found by Hoff who added large numbers of terms to $W(x, y)$ and found that in the limiting case (ie: approaching the Yoshimura pattern) the minimum postbuckling load supported by the cylinder approached zero.

LIST OF PUBLICATIONS AND PAPERS PRESENTED UNDER
NASA RESEARCH GRANT NGR 52-026-(011)

Publications

1. <u>Photoelastic Circular Cylinders in Axial Compression,</u>

   by R. C. Tennyson, Symposium on Test Methods for Compression

   Members, ASTM, 1967.

2. <u>Analysis of the Buckling Process of Circular Cylindrical Shells</u>

   <u>Under Axial Compression,</u>

   by R, C. Tennyson and S. W. Welles, UTIAS Report to be published.

Papers Presented

1. <u>Photoelastic Circular Cylinders in Axial Compression,</u>   .

   Symposium on Test Methods for Compression Members,

   ASTM Annual Meeting, June, 1966.

2. <u>Analysis of the Buckling Process of Circular Cylindrical Shells Under</u>

   <u>Axial Compression,</u>

   Canadian Congress of Applied Mechanics,

   Laval University, May, 1967.
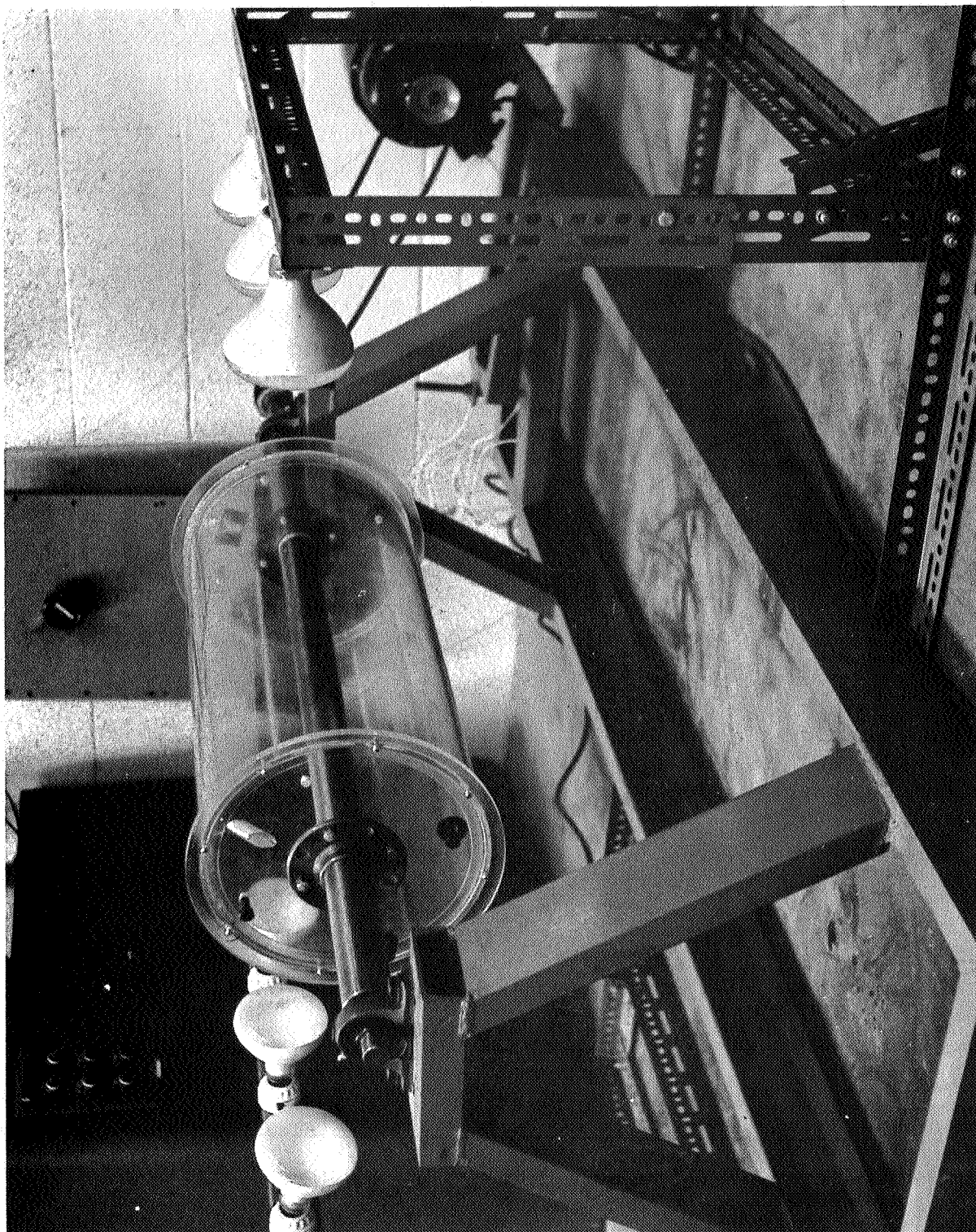
FIG. H-6.1 ROTATION APPARATUS FOR SPE-CASTEG PLASTIC CIRCULAR CYLINDERS
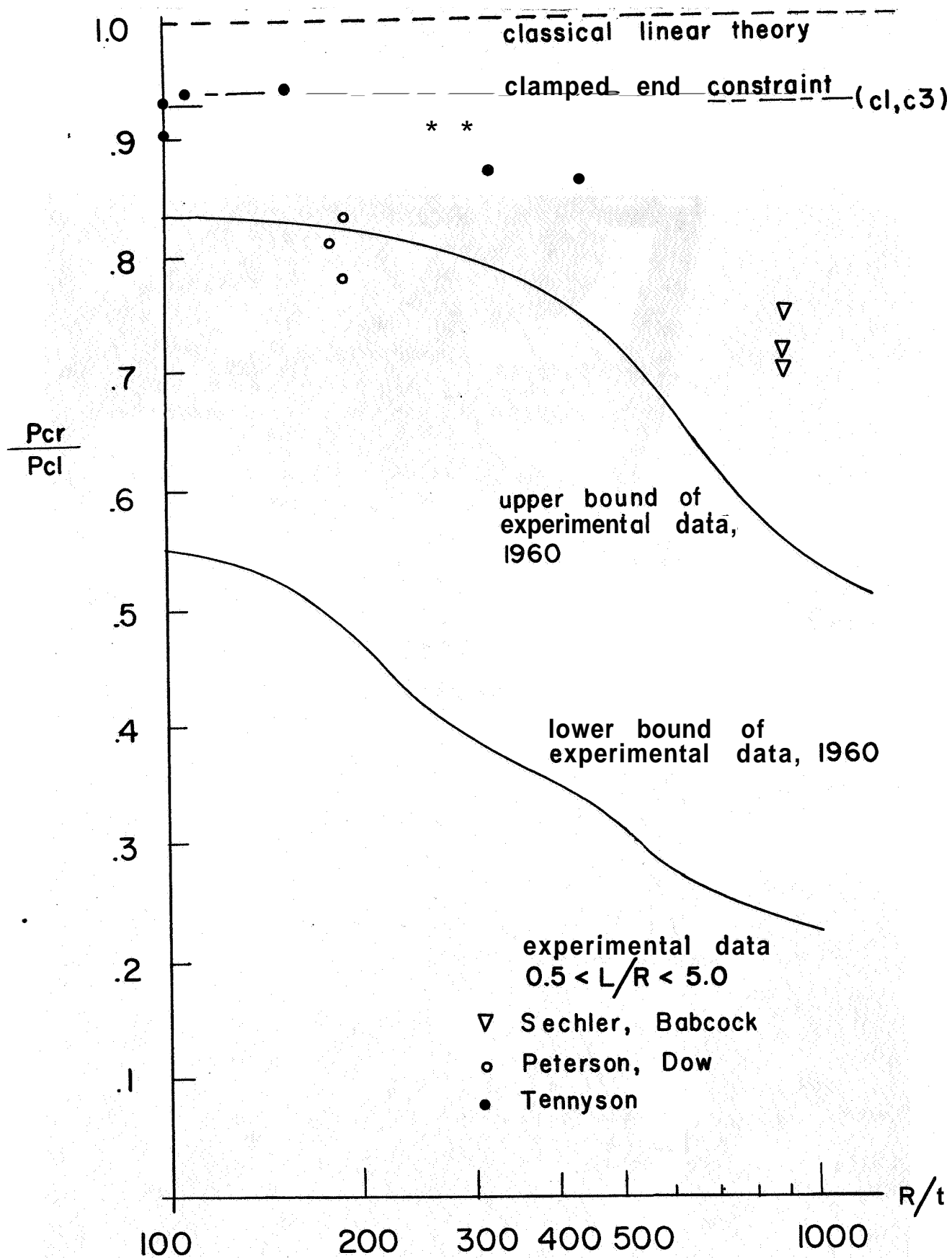
FIG. H-6.2 COMPARISON OF EXPERIMENTAL BUCKLING STRESSES
WITH THEORY FOR CIRCULAR CYLINDRICAL SHELLS
UNDER AXIAL COMPRESSION
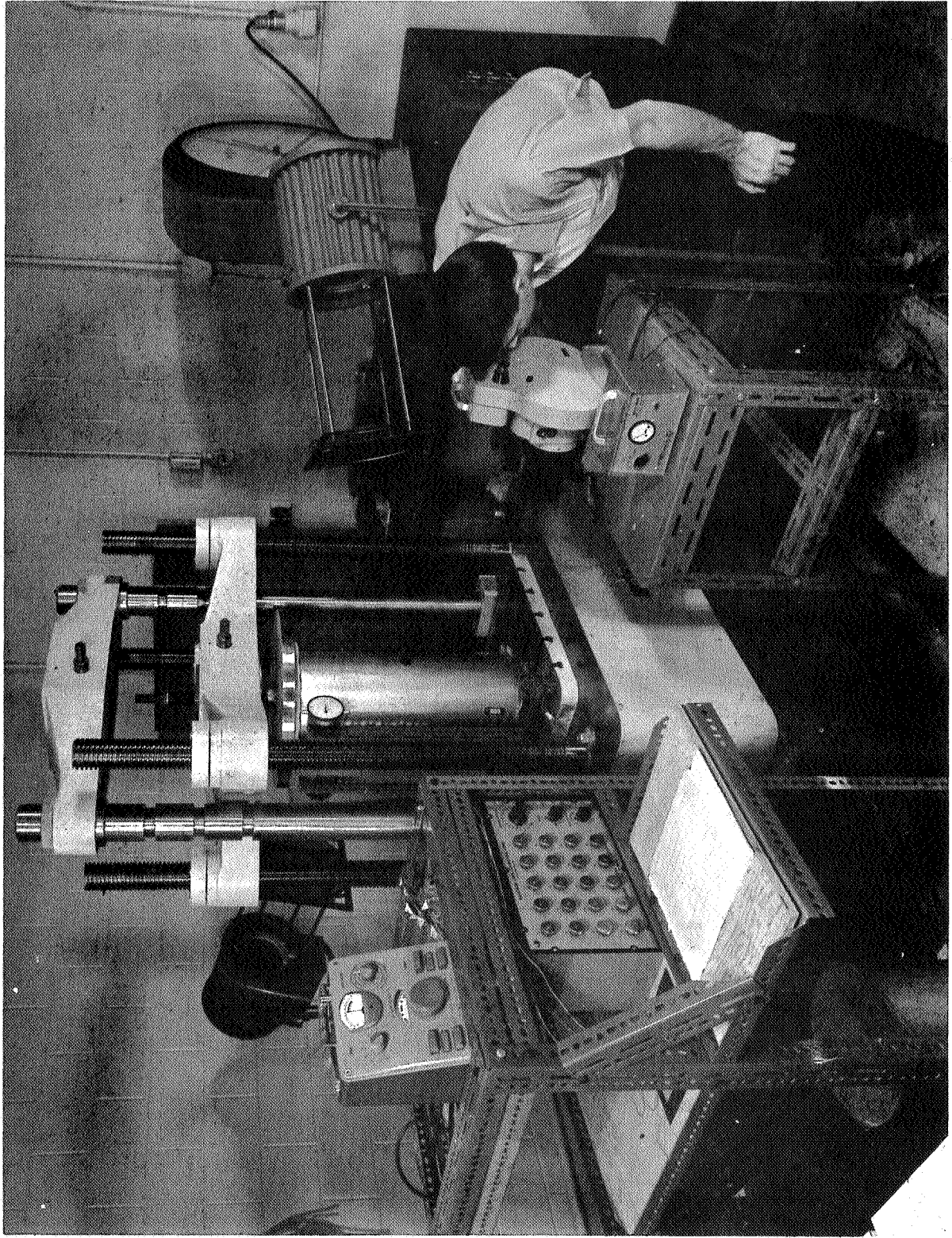
FIG. H-6.3 GENERAL LAYOUT OF TESTING EQUIPMENT

FRAME

1

2

3

4

5

6

7

8

9

1

2

FIG. H-6.4 THE BUCKLING PROCESS AS VIEWED THROUGH A PLANE
REFLECTION POLARISCOPE SET AT 45°
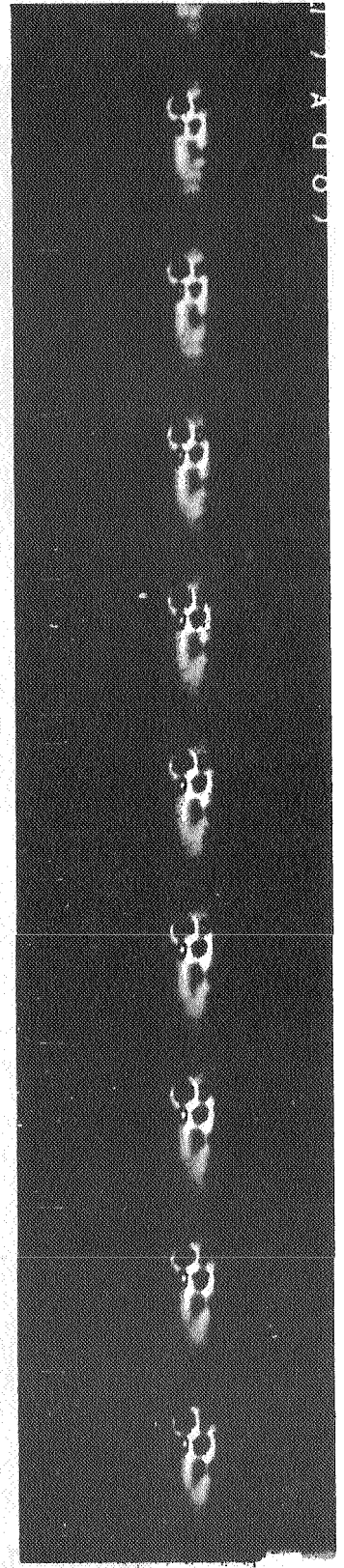
FRAME

1

2

3

4

5

6

7

8

9
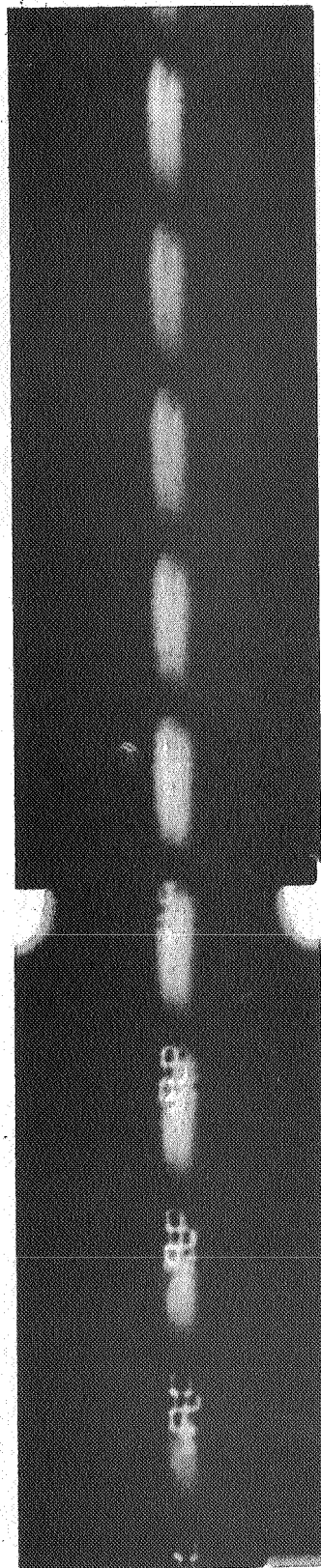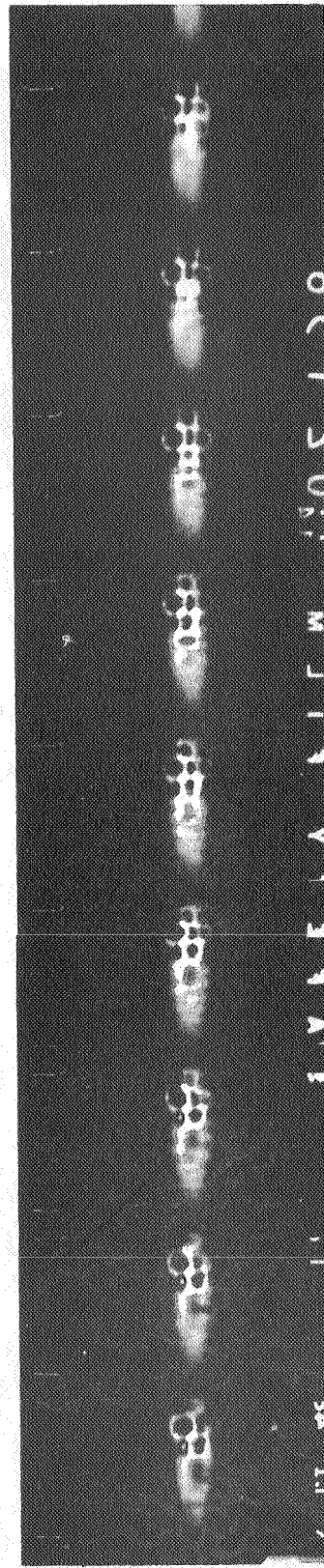
1   2   3

FIG. **H-6.5**   CHANGE IN 45° ISOCLINIC PATTERN OVER ENTIRE CYLINDER
LENGTH DURING BUCKLING PROCESS (INITIAL STAGE)

FRAME

1

2

3

4

5

6

7

8

9
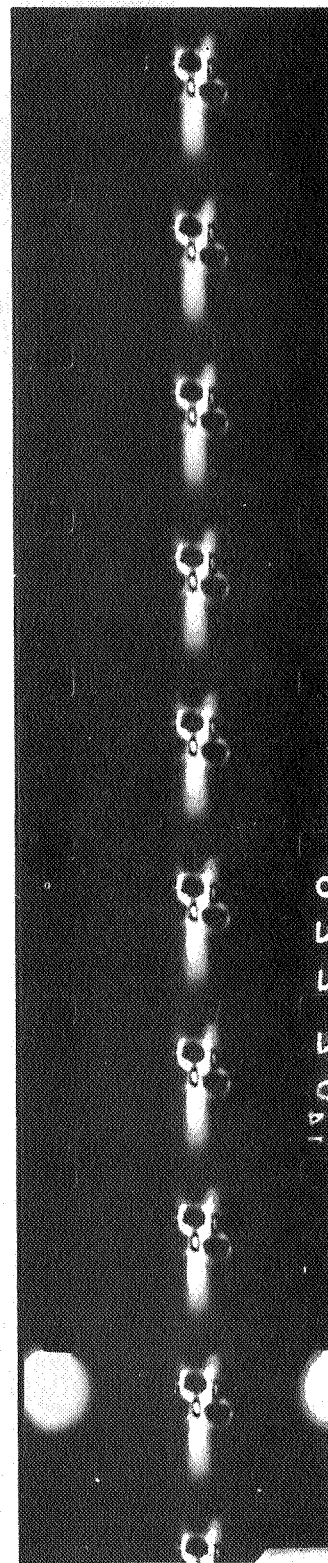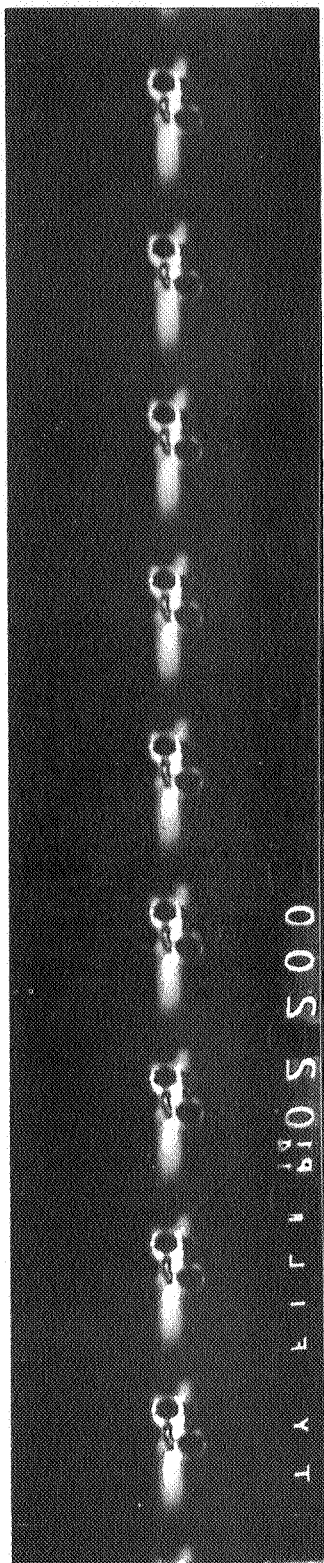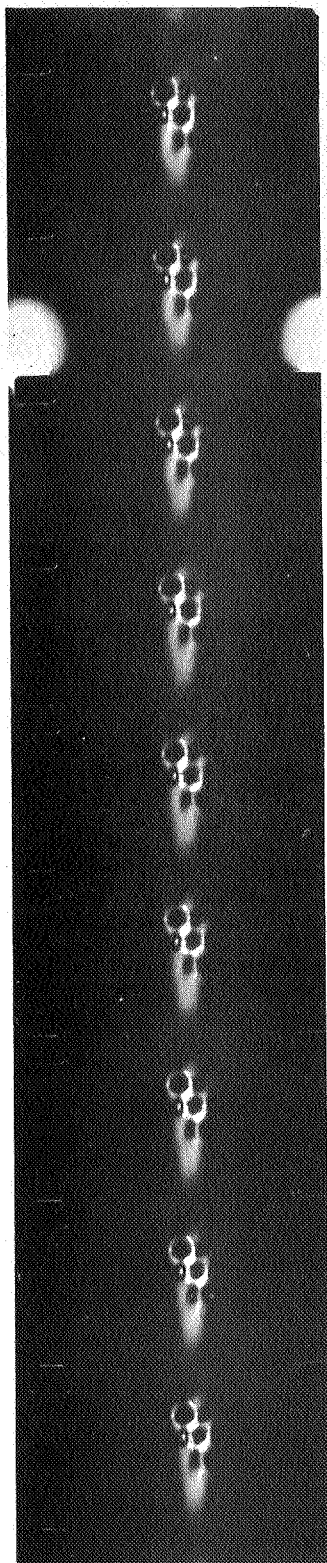
1   2   3

FIG. H-6.6   CHANGE IN 45° ISOCLINIC PATTERN OVER ENTIRE CYLINDER
              LENGTH DURING BUCKLING PROCESS (FINAL STAGE)
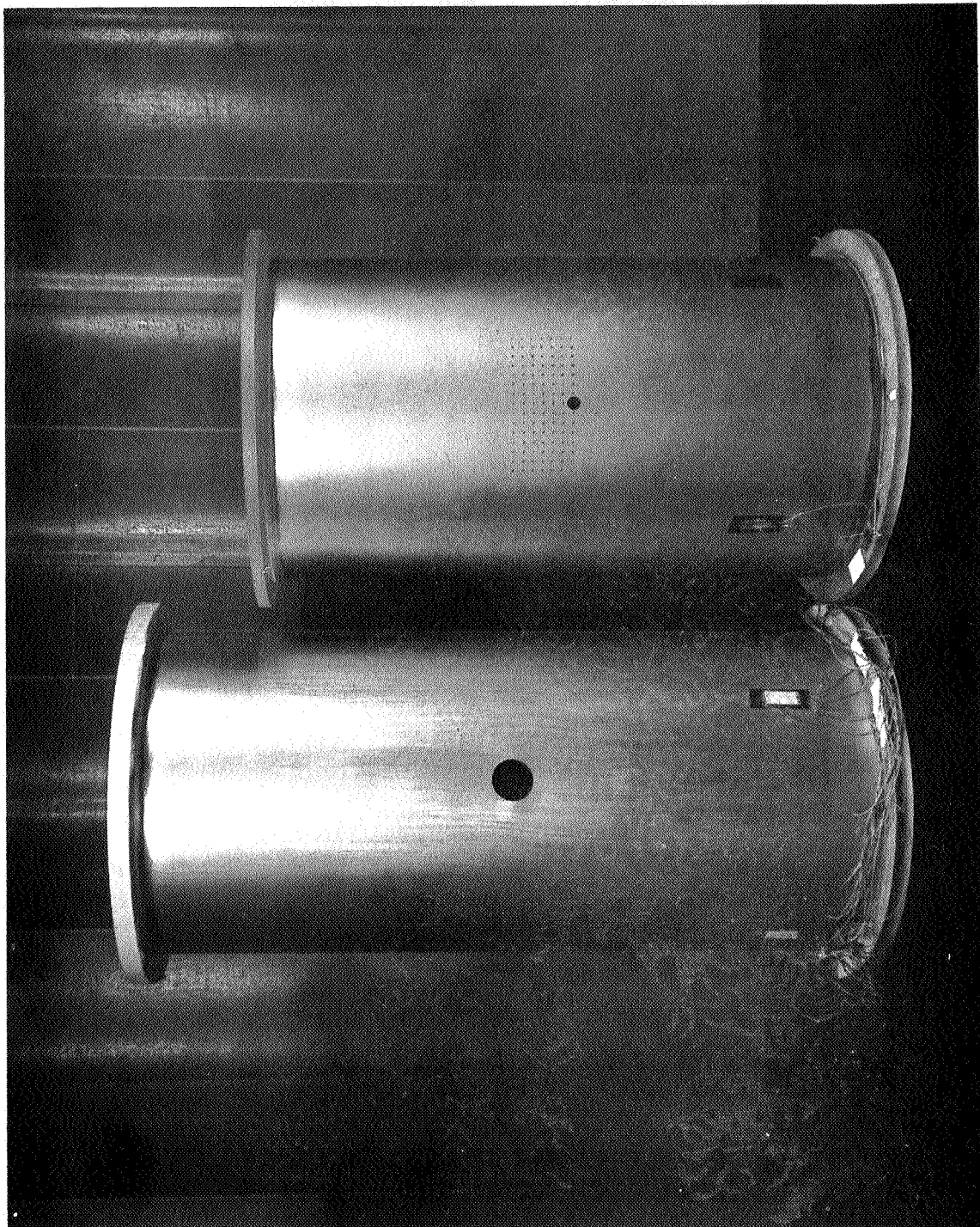
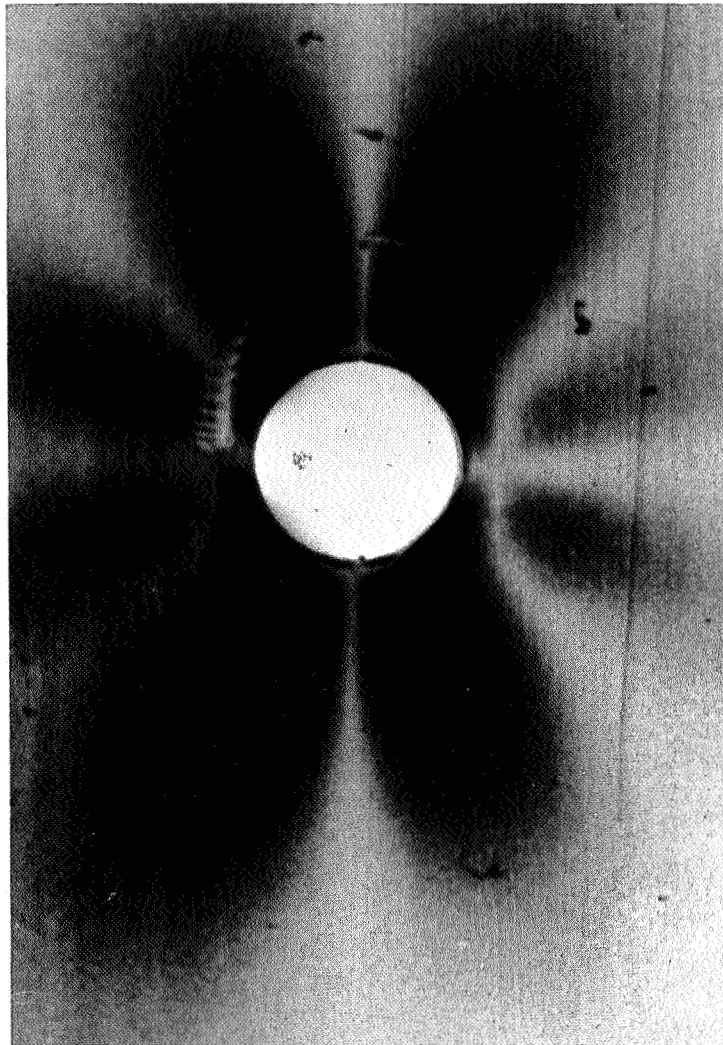FIG. H-7.1 CIRCULAR CUTOUTS IN PHOTOELASTIC PLASTIC CYLINDERS

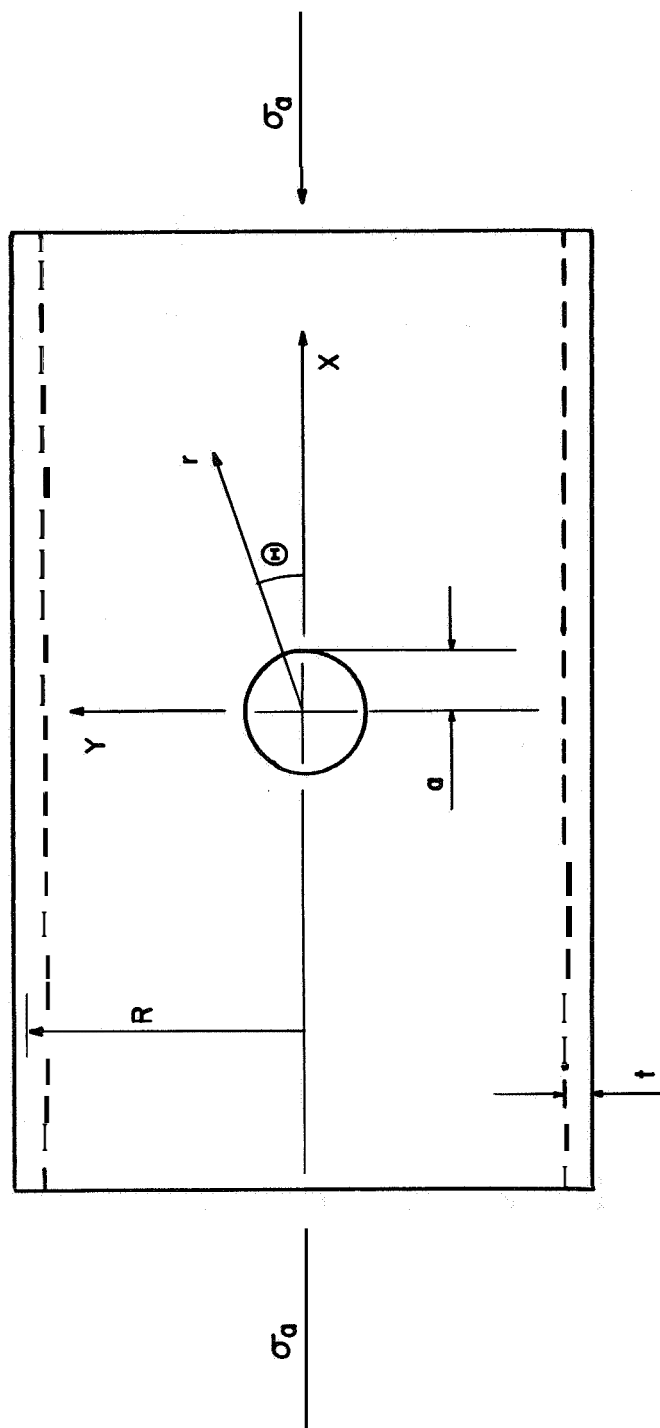FIG. **H-7.2**   0°, 90° ISOCLINIC PATTERNS FOR CIRCULAR HOLE IN
CYLINDER UNDER **AXIAL** COMPRESSION
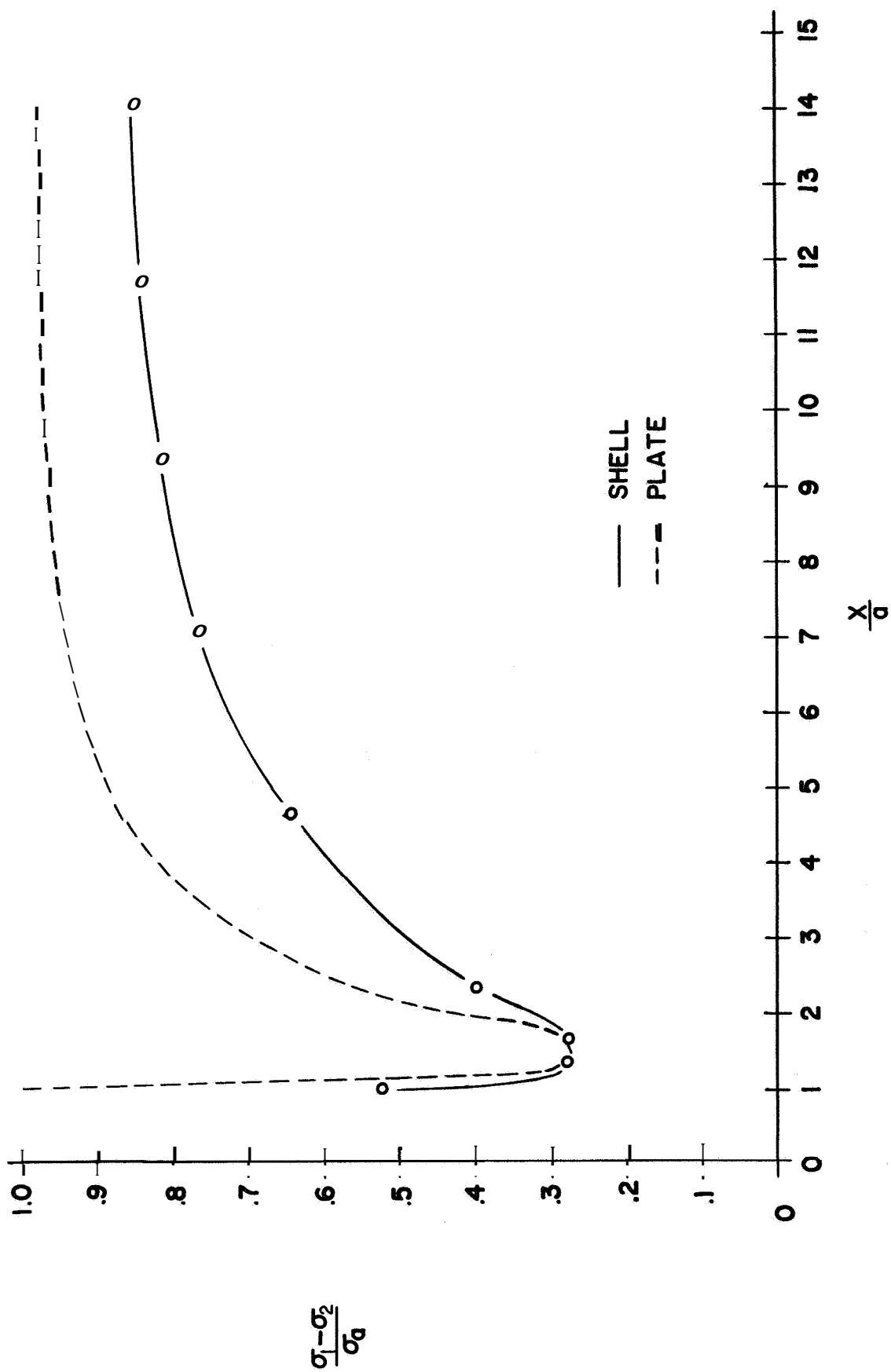
FIG. H-7.3   CYLINDER NOMENCLATURE

FIG. H-7.4   VARIATION OF PRINCIPAL STRESS DIFFERENCE ALONG X-AXIS
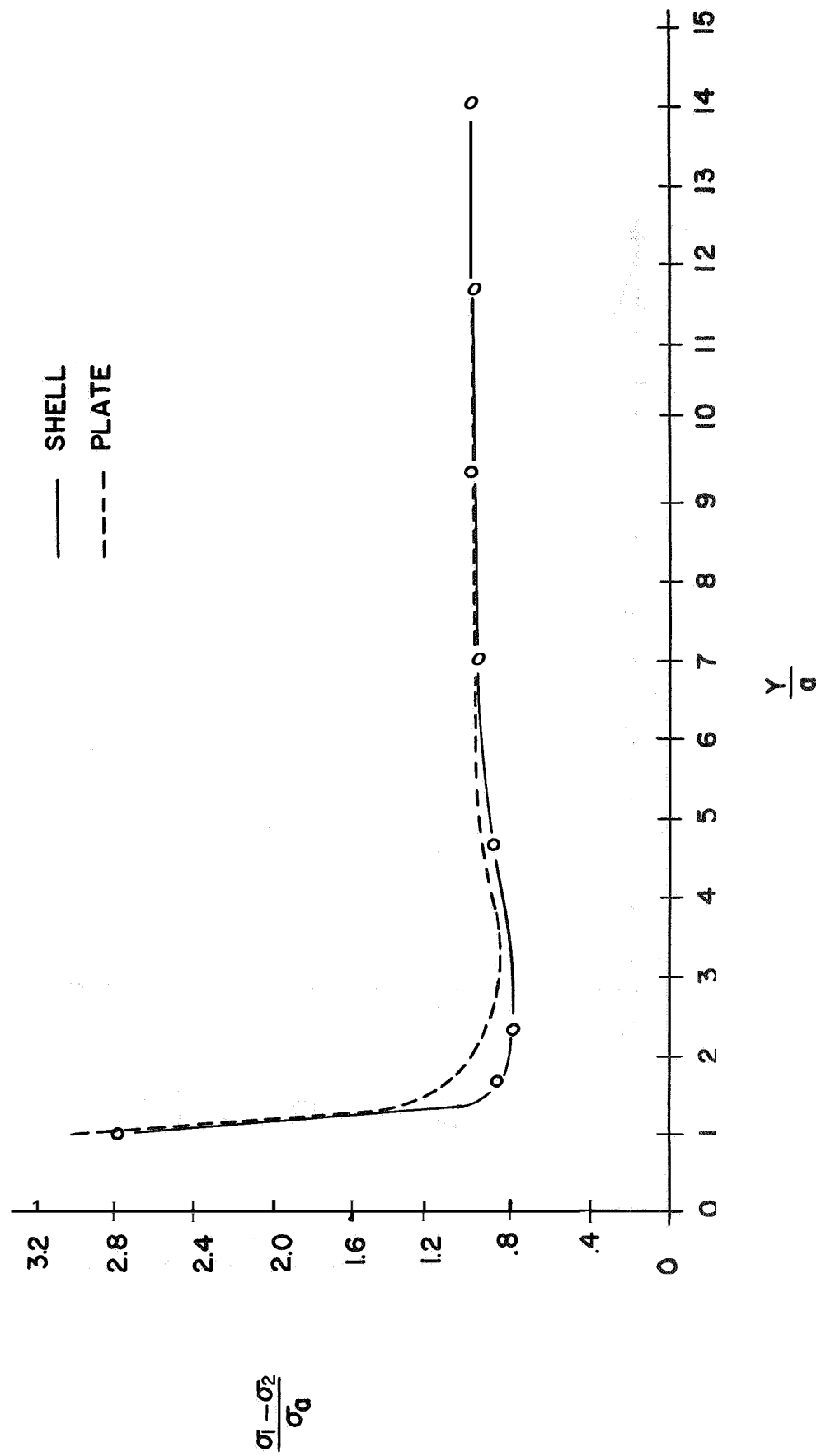AS DETERMINED FROM PHOTOELASTIC MEASUREMENTS

FIG. H-7.5   VARIATION OF PRINCIPAL STRESS DIFFERENCE ALONG Y-AXIS
AS DETERMINED FROM PHOTOELASTIC MEASUREMENTS

$$\beta^2 = a' \left[12 \left(1 - \nu^2 \right) \right]^{1/2} \Big/ 8 \, R \, t$$
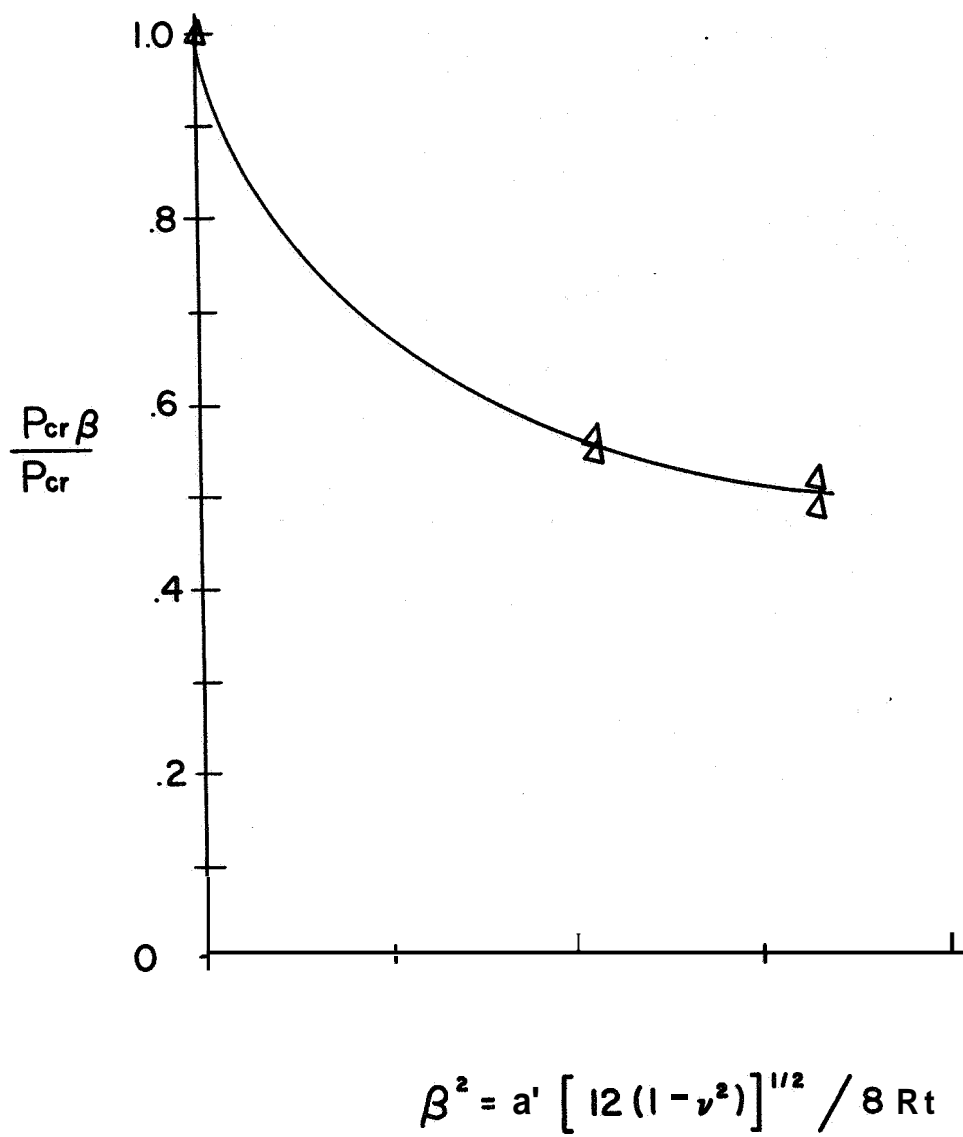
FIG. H-7.6   VARIATION OF CRITICAL BUCKLING STRESS WITH CURVATURE
PARAMETER FOR CYLINDER CONTAINING A CIRCULAR CUTOUT